



Aaij, R. et al. (2014) Measurement of the charge asymmetry in $B^\pm \rightarrow \phi K^\pm$ and search for $B^\pm \rightarrow \phi \pi^\pm$ decays. Physics Letters B, 728, pp. 85-94.

Copyright © 2014 The Authors.

This work is made available under the Creative Commons Attribution 3.0 Unported License (CC BY 3.0).

Version: Published

<http://eprints.gla.ac.uk/106839/>

Deposited on: 29 May 2015

Enlighten – Research publications by members of the University of Glasgow <http://eprints.gla.ac.uk>



Measurement of the charge asymmetry in $B^\pm \rightarrow \phi K^\pm$ and search for $B^\pm \rightarrow \phi \pi^\pm$ decays



LHCb Collaboration

ARTICLE INFO

Article history:

Received 18 September 2013
 Received in revised form 18 November 2013
 Accepted 18 November 2013
 Available online 22 November 2013
 Editor: W.-D. Schlatter

ABSTRACT

The CP -violating charge asymmetry in $B^\pm \rightarrow \phi K^\pm$ decays is measured in a sample of pp collisions at 7 TeV centre-of-mass energy, corresponding to an integrated luminosity of 1.0 fb^{-1} collected by the LHCb experiment. The result is $\mathcal{A}_{CP}(B^\pm \rightarrow \phi K^\pm) = 0.022 \pm 0.021 \pm 0.009$, where the first uncertainty is statistical and the second systematic. In addition, a search for the $B^\pm \rightarrow \phi \pi^\pm$ decay mode is performed, using the $B^\pm \rightarrow \phi K^\pm$ decay rate for normalization. An upper limit on the branching fraction $\mathcal{B}(B^\pm \rightarrow \phi \pi^\pm) < 1.5 \times 10^{-7}$ is set at 90% confidence level.

© 2013 The Authors. Published by Elsevier B.V. Open access under CC BY license.

1. Introduction

The weak-interaction $B^\pm \rightarrow \phi K^\pm$ decay is governed by the $b \rightarrow ss\bar{s}$ transition. In the Standard Model (SM), it can only occur through loop diagrams (see Fig. 1), leading to a branching fraction of order 10^{-5} [1]. Because the dominant amplitudes have similar weak phases, the CP -violating charge asymmetry, defined as

$$\mathcal{A}_{CP}(B^\pm \rightarrow \phi K^\pm) \equiv \frac{\mathcal{B}(B^- \rightarrow \phi K^-) - \mathcal{B}(B^+ \rightarrow \phi K^+)}{\mathcal{B}(B^- \rightarrow \phi K^-) + \mathcal{B}(B^+ \rightarrow \phi K^+)}, \quad (1)$$

is predicted to be small in the SM, typically 1–2% with uncertainties of a few percent [2,3]. A significantly larger value would signal interference with an amplitude not described in the SM. The current experimental world average is $\mathcal{A}_{CP}(B^\pm \rightarrow \phi K^\pm) = 0.10 \pm 0.04$ [1], dominated by a recent measurement from the BaBar Collaboration [4]. Large CP violation effects have been seen in some regions of the $B^\pm \rightarrow K^+ K^- K^\pm$ phase space, but not around the ϕ resonance [5].

The $B^\pm \rightarrow \phi \pi^\pm$ decay is another flavour-changing neutral current process, driven by the $b \rightarrow ds\bar{s}$ quark-level transition (see Fig. 1). The high suppression, due to the tiny product of the Cabibbo–Kobayashi–Maskawa matrix elements [6,7] and to the Okubo–Zweig–Iizuka (OZI) rule [8–10] associated with the creation of the colourless $s\bar{s}$ pair forming the ϕ meson, makes this rare loop decay a sensitive probe of the SM. Indeed, even a small non-SM amplitude, e.g. from R-parity violating supersymmetry [11], may dominate over the SM contribution.

The current SM prediction for the $B^\pm \rightarrow \phi \pi^\pm$ branching fraction suffers from uncertainties originating from the naïve factor-

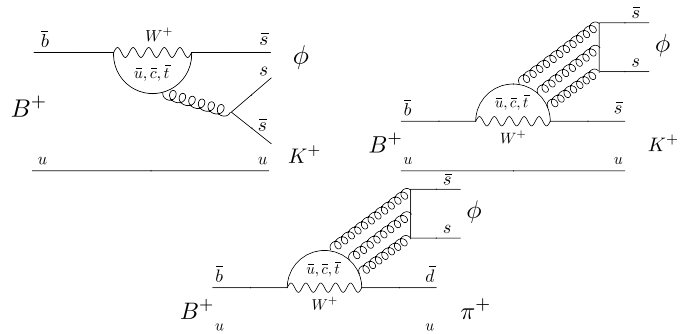


Fig. 1. Lowest-order Feynman diagrams of the Standard Model for the decays $B^+ \rightarrow \phi K^+$ (top) and $B^+ \rightarrow \phi \pi^+$ (bottom). The diagrams with an external ϕ meson are OZI suppressed.

ization approach, radiative corrections, calculation of the long-distance contribution (e.g. $B \rightarrow KK^*$ rescattering), and ω - ϕ mixing [12]. The latter is the main source of uncertainty. The physical ω and ϕ meson states do not coincide exactly with the ideal $(|u\bar{u}\rangle + |d\bar{d}\rangle)/\sqrt{2}$ and $|s\bar{s}\rangle$ states, respectively. They appear to be mixtures of these two states characterized by a small mixing angle δ_V [13,14], which depends on the magnitude of SU(3) symmetry breaking and can be determined in the framework of chiral perturbation theory. However, more sophisticated treatments based on the full ρ^0 - ω - ϕ mixing scheme suggest that δ_V is mass dependent, i.e. takes different values at the ω and ϕ masses [15,16]. In the QCD factorization approach, the $B^\pm \rightarrow \phi \pi^\pm$ branching fraction is predicted to be in the range $(5 - 10) \times 10^{-9}$ [3] if ω - ϕ mixing is neglected, but can be enhanced up to 0.6×10^{-7} [12,17] depending on the value of δ_V . However, the effect of ω - ϕ mixing has not been observed in a recent search for $B^0 \rightarrow J/\psi \phi$ [18]. Values of the $B^\pm \rightarrow \phi \pi^\pm$ branching fraction in excess of 10^{-7} would be indicative of non-SM physics.

The $B^\pm \rightarrow \phi\pi^\pm$ decay mode has not been observed yet. Currently, the most stringent experimental limit is $\mathcal{B}(B^\pm \rightarrow \phi\pi^\pm) < 2.4 \times 10^{-7}$ at 90% confidence level (CL), obtained by the BaBar Collaboration [19].

This Letter presents a measurement of the $B^\pm \rightarrow \phi K^\pm$ charge asymmetry and a search for the $B^\pm \rightarrow \phi\pi^\pm$ decay mode with the LHCb detector. The results are based on a data sample collected during the 2011 pp run of the Large Hadron Collider at a centre-of-mass energy of 7 TeV, corresponding to an integrated luminosity of 1.0 fb^{-1} . The ϕ meson is reconstructed in the K^+K^- final state. We define the ϕ signal as any peaking component in the K^+K^- mass spectrum consistent with the known parameters of the ϕ resonance, without attempting a full amplitude analysis of the three-body $K^+K^-K^\pm$ and $K^+K^-\pi^\pm$ final states. In order to suppress several systematic effects, the primary observables measured in this analysis are the difference of CP -violating charge asymmetries

$$\Delta\mathcal{A}_{CP} \equiv \mathcal{A}_{CP}(B^\pm \rightarrow \phi K^\pm) - \mathcal{A}_{CP}(B^\pm \rightarrow J/\psi K^\pm), \quad (2)$$

and the branching fraction ratio $\mathcal{B}(B^\pm \rightarrow \phi\pi^\pm)/\mathcal{B}(B^\pm \rightarrow \phi K^\pm)$, which are then converted to results on $\mathcal{A}_{CP}(B^\pm \rightarrow \phi K^\pm)$ and $\mathcal{B}(B^\pm \rightarrow \phi\pi^\pm)$ using the best known values of $\mathcal{A}_{CP}(B^\pm \rightarrow J/\psi K^\pm)$ [1,20] and $\mathcal{B}(B^\pm \rightarrow \phi K^\pm)$ [1]. The choice of $B^\pm \rightarrow J/\psi K^\pm$ as reference channel and other features of the analysis follow the approach adopted in inclusive studies of $B^\pm \rightarrow K^+K^-K^\pm$ decays with the same data set [5].

The two measurements are performed in a common analysis, *i.e.* they are based on identical event selections and data descriptions whenever possible. The observables are obtained from two-dimensional maximum likelihood fits to the unbinned B^\pm and ϕ mass distributions of the reconstructed candidates, using parametric shapes with minimal dependence on simulation. The results of these fits were not examined until the entire analysis procedure was finalized.

2. Detector and data set

The LHCb detector [21] is a single-arm forward spectrometer covering the pseudorapidity range $2 < \eta < 5$, designed for the study of particles containing b or c quarks. The detector includes a high-precision tracking system consisting of a silicon-strip vertex detector surrounding the pp interaction region, a large-area silicon-strip detector located upstream of a dipole magnet with a bending power of about 4 Tm, and three stations of silicon-strip detectors and straw drift tubes placed downstream. The combined tracking system provides a momentum measurement with a relative uncertainty that varies from 0.4% at 5 GeV/c to 0.6% at 100 GeV/c, and an impact parameter (IP) resolution of 20 μm for tracks with high transverse momentum (p_T). Charged hadrons are identified using two ring-imaging Cherenkov detectors [22]. Photon, electron and hadron candidates are identified by a calorimeter system consisting of scintillating-pad and preshower detectors, an electromagnetic calorimeter and a hadronic calorimeter. Muons are identified by a system composed of alternating layers of iron and multiwire proportional chambers. The direction of the magnetic field of the spectrometer dipole magnet is reversed regularly.

The trigger [23] consists of a hardware stage, based on information from the calorimeter and muon systems, followed by a software stage, which applies a full event reconstruction. The B^\pm candidate decays considered in this analysis must belong to one of two exclusive categories of events, called TOS (triggered on signal) or TIS (triggered independently of signal). A TOS event is triggered at the hardware stage by one of the candidate's final-state particles being compatible with a transverse energy deposit greater

than 3.5 GeV in the hadron calorimeter. A TIS event does not satisfy the TOS definition and is triggered at the hardware stage by activity in the rest of the event. All candidates must pass a software trigger requiring a two-, three- or four-track secondary vertex with a large scalar sum of the transverse momentum of the tracks and a significant displacement from the primary pp interaction vertices (PVs). At least one track should have $p_T > 1.7 \text{ GeV}/c$ and χ_{IP}^2 with respect to any PV greater than 16, where χ_{IP}^2 is defined as the difference in χ^2 of a given PV reconstructed with and without the considered track. A multivariate algorithm [24] is used for the identification of secondary vertices consistent with the decay of a b hadron.

In the simulation, pp collisions are generated using PYTHIA 6.4 [25] with a specific LHCb configuration [26]. Decays of hadronic particles are described by EVTGEN [27], in which final state radiation is generated using PHOTOS [28]. The interaction of the generated particles with the detector and its response are implemented using the GEANT4 toolkit [29] as described in Ref. [30].

3. Event selection and efficiency

The selections of $B^\pm \rightarrow \phi K^\pm$ and $B^\pm \rightarrow \phi\pi^\pm$ candidates are identical, except for the particle identification (PID) requirement on the charged hadron combined with the ϕ candidate, which is referred to as the bachelor hadron h^\pm ($h^\pm = K^\pm$ or π^\pm). The other requirements are chosen to minimize the relative statistical uncertainty on the $B^\pm \rightarrow \phi K^\pm$ signal yield.

Only good quality tracks with $\chi_{IP}^2 > 25$ and $p_T > 0.25 \text{ GeV}/c$ are used in the reconstruction. The ϕ meson candidates are reconstructed from two oppositely-charged tracks identified as kaons with the PID requirement $\text{DLL}_{K\pi} > 2$, where $\text{DLL}_{K\pi}$ is the difference in log-likelihood between the kaon and pion hypotheses, as determined with the ring-imaging Cherenkov detectors in control samples of known particle composition [22]. The ϕ candidates are required to have $p_T > 2 \text{ GeV}/c$, a total momentum, p , larger than 10 GeV/c and an invariant mass, $m_{K\bar{K}}$, in the range 1.00–1.05 GeV/c². Bachelor hadrons, reconstructed either as pions if $\text{DLL}_{K\pi} < -1$ or kaons otherwise, are required to have $p > 10 \text{ GeV}/c$ and $p_T > 2.5 \text{ GeV}/c$, and are combined with ϕ candidates to form $B^\pm \rightarrow \phi h^\pm$ candidates. These B^\pm candidates are required to have $p_T > 2 \text{ GeV}/c$, a three-track vertex χ^2 per degree of freedom less than 9, and an invariant mass $m_{K\bar{K}h}$ in the range 5.0–5.5 GeV/c². Furthermore $\cos\theta_p$ is required to be greater than 0.9999, where θ_p is the angle between the B^\pm momentum vector and the vector joining the B^\pm production vertex to the B^\pm decay vertex. The production vertex is chosen as the PV for which the B^\pm has the smallest χ_{IP}^2 .

Multiple candidates, occurring in 0.2% of the events, are removed by keeping the candidate with the smallest B^\pm vertex χ^2 . The final data sample consists of 6251 $B^\pm \rightarrow \phi K^\pm$ candidates and 2169 $B^\pm \rightarrow \phi\pi^\pm$ candidates.

The PID performance is determined from a large and high-purity sample of pions from prompt $D^{*+} \rightarrow D^0(K^-\pi^+)\pi^+$ and $D^{*-} \rightarrow \bar{D}^0(K^+\pi^-)\pi^-$ decays, as a function of p and η . After reweighting this calibration sample to the same momentum and pseudorapidity distributions as for the bachelor pion in simulated $B^\pm \rightarrow \phi\pi^\pm$ decays, the efficiency of the PID requirement $\text{DLL}_{K\pi} < -1$ for the bachelor pion is measured to be $0.846 \pm 0.011(\text{stat}) \pm 0.020(\text{syst})$, with a 5% kaon misidentification probability. All other efficiencies, which are slightly different for $B^\pm \rightarrow \phi\pi^\pm$ and $B^\pm \rightarrow \phi K^\pm$ decays due to their kinematic properties, are determined from simulation. The efficiency ratio

$$\frac{\epsilon(B^\pm \rightarrow \phi\pi^\pm)}{\epsilon(B^\pm \rightarrow \phi K^\pm)} = 0.762 \pm 0.031(\text{stat}) \pm 0.036(\text{syst}) \quad (3)$$

is obtained, where the numerator is the total efficiency for a $B^\pm \rightarrow \phi\pi^\pm$ decay to be selected as a $B^\pm \rightarrow \phi\pi^\pm$ candidate and the denominator is the total efficiency for a $B^\pm \rightarrow \phi K^\pm$ decay to be selected either as a $B^\pm \rightarrow \phi K^\pm$ candidate or as a $B^\pm \rightarrow \phi\pi^\pm$ candidate. The statistical uncertainty arises from the size of the calibration and simulation samples, while the systematic uncertainty is the quadratic sum of contributions from the PID (± 0.018), the trigger (± 0.008), and other offline kinematic selection requirements (± 0.030).

4. Fit description

The observables of interest, namely the asymmetry between the $B^- \rightarrow \phi K^-$ and $B^+ \rightarrow \phi K^+$ yields and the ratio between the $B^\pm \rightarrow \phi\pi^\pm$ and $B^\pm \rightarrow \phi K^\pm$ yields, are each determined from a two-dimensional unbinned extended maximum likelihood fit based on probability density functions (PDFs) of the m_{KKh} and m_{KK} masses. In each case, independent subsamples of events, each with either $B^\pm \rightarrow \phi K^\pm$ candidates or $B^\pm \rightarrow \phi\pi^\pm$ candidates, are fitted simultaneously. For each subsample, the likelihood is written as

$$\mathcal{L} = \exp\left(-\sum_j N_j\right) \prod_i \left(\sum_j N_j P_j^i\right), \quad (4)$$

where N_j is the yield of fit component j , P_j^i is the probability of event i for component j , and the index i runs over the N events in the subsample. Except for the misidentified components described further below, the probabilities P_j^i are given by the product of PDFs for the two $K^+K^-h^\pm$ and K^+K^- invariant masses, evaluated at the values m_{KKh}^i and m_{KK}^i of event i :

$$P_j^i = P_j^{KKh}(m_{KKh}^i) P_j^{KK}(m_{KK}^i). \quad (5)$$

This assumes that the two mass variables are independent, as supported by data and simulation studies. The correlation between m_{KKh} and m_{KK} is found to be less than 4%.

The description of the m_{KKh} distributions involves a combination of three contributions: a signal peaking at the B^\pm mass, a broad low-mass background with an end-point near 5150 MeV/ c^2 due to partially-reconstructed b -hadron decays such as $B^0 \rightarrow \phi K^{*0}$, and a linear background from random combinations. The peaking signal is modelled with a Crystal Ball function [31] modified such that both the upper and lower tails are power laws. The mean and the width σ_B of the Crystal Ball function are free in the fit, while the tail parameters are determined from simulation. The partially-reconstructed background is described with an ARGUS function [32] convoluted with a Gaussian resolution function of the same σ_B as the B^\pm signal. The m_{KK} distribution is described with two contributions: a peaking term centred on the ϕ mass, described with a relativistic Breit–Wigner function convoluted with a Gaussian resolution function of free width, and a linear term originating from nonresonant, S -wave, or random combinations of two kaons. The above three m_{KKh} contributions and two m_{KK} contributions lead to six components for each subsample: the $B^\pm \rightarrow \phi h^\pm$ signal, the nonresonant $B^\pm \rightarrow K^+K^-h^\pm$ background, the partially-reconstructed b -hadron backgrounds with or without a true ϕ meson (for example $B \rightarrow \phi h^\pm\pi$ or $B \rightarrow K^+K^-h^\pm\pi$), and the combinatorial backgrounds with or without a true ϕ meson. The nonresonant $B^\pm \rightarrow K^+K^-h^\pm$ components include $b \rightarrow c$ decays, which are found to be negligible from simulation studies.

In addition, we consider components for the misidentified $B^\pm \rightarrow \phi K^\pm$ and $B^\pm \rightarrow K^+K^-K^\pm$ decays in the $B^\pm \rightarrow \phi\pi^\pm$ sample, while misidentified $B^\pm \rightarrow \phi\pi^\pm$ and $B^\pm \rightarrow K^+K^-K^\pm$ decays

in the $B^\pm \rightarrow \phi K^\pm$ sample are negligible, and therefore ignored. For these two additional components, the $m_{KK\pi}$ PDF is conditional to the observable $\delta m = m_{KKK} - m_{KK\pi}$, which is the mass difference under the two bachelor hadron mass hypotheses. The probabilities are written as

$$P_j^i = P_{\text{misID}}^{KK\pi}(m_{KK\pi}^i|\delta m^i) P_j^{KK}(m_{KK}^i), \quad (6)$$

where P_j^{KK} is the m_{KK} PDF described above (representing either ϕ signal or background) and

$$P_{\text{misID}}^{KK\pi}(m_{KK\pi}^i|\delta m^i) = P_{\phi K}^{KKK}(m_{KK\pi}^i + \delta m^i)|_{\sigma_B \rightarrow \rho\sigma_B}. \quad (7)$$

Here $P_{\phi K}^{KKK}$ is the m_{KKK} PDF of the $B^\pm \rightarrow \phi K^\pm$ signal, but with an increased B^\pm mass resolution to account for the effects of the typically higher momentum of misidentified bachelor kaons. The parameter σ_B is multiplied here by the central value of a factor $\rho = 1.26 \pm 0.10$, determined from data as the ratio of the measured m_{KKK} resolutions of the $B^\pm \rightarrow \phi K^\pm$ signal in the regions $-7 < \text{DLL}_{K\pi} < -1$ and $\text{DLL}_{K\pi} > -1$. The expression in Eq. (7) is equivalent to $P_{\phi K}^{KKK}(m_{KKK}^i)|_{\sigma_B \rightarrow \rho\sigma_B}$, which means that the $B^\pm \rightarrow \phi K^\pm$ misidentified component in the $B^\pm \rightarrow \phi\pi^\pm$ sample would have a $B^\pm \rightarrow \phi K^\pm$ signal distribution if the correct mass was assigned to the bachelor kaon. The advantage of introducing the δm observable is to connect the $B^\pm \rightarrow \phi K^\pm$ shapes in the $B^\pm \rightarrow \phi\pi^\pm$ and $B^\pm \rightarrow \phi K^\pm$ samples, thereby constraining the misidentified $B^\pm \rightarrow \phi K^\pm$ component in the $B^\pm \rightarrow \phi\pi^\pm$ sample using the large signal in the $B^\pm \rightarrow \phi K^\pm$ sample. This procedure allows to describe the misidentified component with the same parametric shape as the $B^\pm \rightarrow \phi\pi^\pm$ signal, and reduces the statistical uncertainty on the $B^\pm \rightarrow \phi\pi^\pm$ yield by a factor of two. However, this introduces a bias because the δm distribution, which is not accounted for in the likelihood, is not the same for all components [33]. To reduce this bias, the $B^\pm \rightarrow \phi\pi^\pm$ sample is divided into four bins of δm , each with its own eight components. This procedure reduces the bias on the $B^\pm \rightarrow \phi\pi^\pm$ signal yield to a negligible level.

Other fit parameters that are common to the different subsamples are the m_{KKh} end-point of the partially-reconstructed backgrounds, the peaking m_{KK} PDF parameters for all components containing a ϕ meson, and the m_{KK} slope of the nonresonant $B^\pm \rightarrow K^+K^-h^\pm$ components. Finally, the ratio of the yield of the misidentified nonresonant $B^\pm \rightarrow K^+K^-K^\pm$ background to the yield of misidentified $B^\pm \rightarrow \phi K^\pm$ background in the $B^\pm \rightarrow \phi\pi^\pm$ sample is constrained to the yield ratio of the corresponding correctly-identified components in the $B^\pm \rightarrow \phi K^\pm$ sample.

The fit procedure is validated on simulated data containing the expected proportion of signal and background events.

These studies, which take into account the different δm distributions and the possible correlation between the fit observables, demonstrate the stability of the fit and show that the fit results are unbiased.

5. Measurement of the $B^\pm \rightarrow \phi K^\pm$ charge asymmetry

The charge asymmetry of the $B^\pm \rightarrow \phi K^\pm$ signal is determined from a fit to the $B^- \rightarrow \phi K^-$ and $B^+ \rightarrow \phi K^+$ candidates in the $\text{DLL}_{K\pi} > -1$ region. These two samples are each divided into two subsamples according to whether the events were TOS or TIS at the hardware trigger stage. In the fit, each of the six components has therefore four yields. For the signal component, they are expressed as $N_{\text{TOS}}^\pm = N_{\text{TOS}}(1 \mp \mathcal{A}_{\text{raw,TOS}})/2$ and $N_{\text{TIS}}^\pm = N_{\text{TIS}}(1 \mp \mathcal{A}_{\text{raw,TIS}})/2$, where N_k is the total yield and $\mathcal{A}_{\text{raw},k}$ is the raw yield asymmetry in subsample k ($k = \text{TOS, TIS}$). The fit has a total of 34 free parameters: 10 mass shape parameters, 12 yields and 12 raw asymmetries.

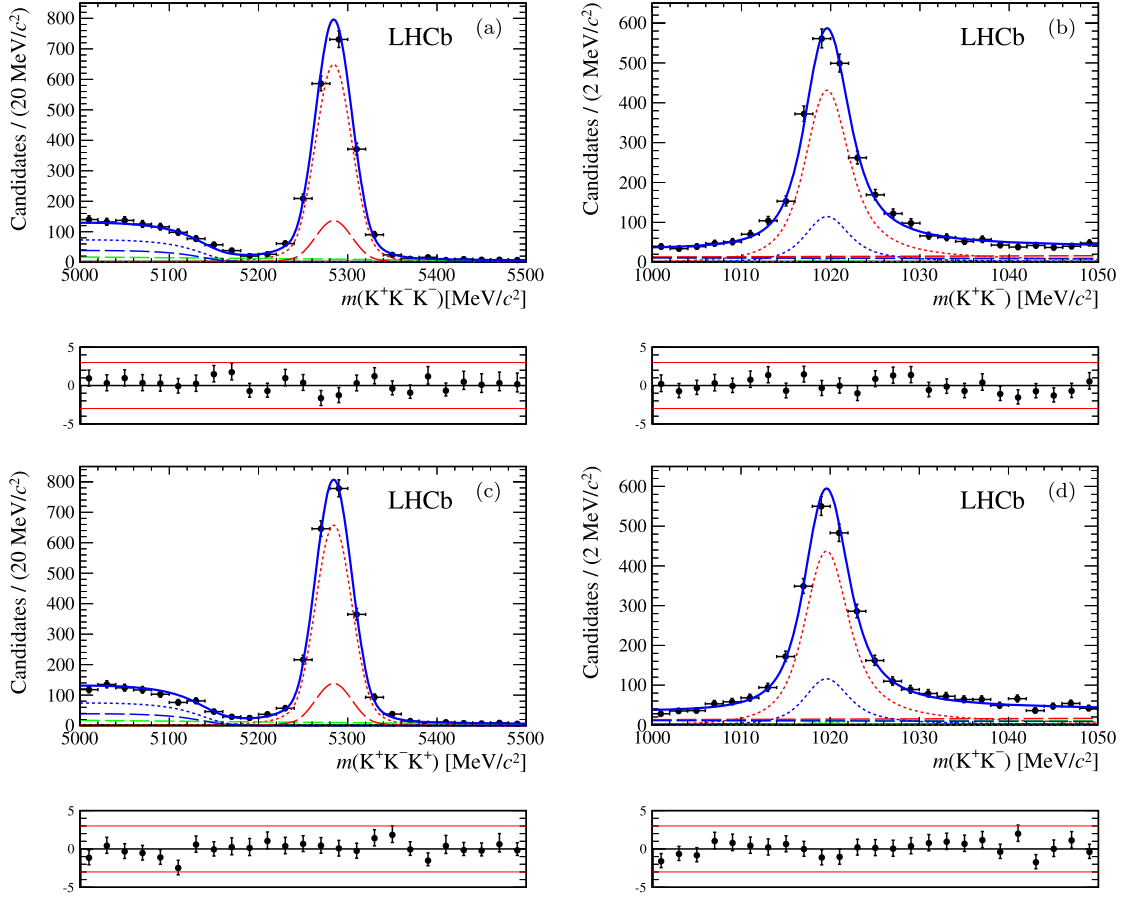


Fig. 2. Distributions of the (a) $K^+K^-K^-$ and (b) K^+K^- masses of the selected $B^- \rightarrow \phi K^-$ candidates, as well as of the (c) $K^+K^-K^+$ and (d) K^+K^- masses of the selected $B^+ \rightarrow \phi K^+$ candidates. The solid blue curves represent the result of the simultaneous fit described in the text, with the following components: $B^\pm \rightarrow \phi K^\pm$ signal (dotted red), nonresonant $B^\pm \rightarrow K^+K^-K^\pm$ background (dashed red), partially-reconstructed b -hadron background with (dotted blue) or without (dashed blue) a true ϕ meson, and combinatorial background with (dotted green) or without (dashed green) a true ϕ meson. Some of the components are barely visible because the corresponding yields are small. Normalized residuals are displayed below each histogram. (For interpretation of the references to colour in this figure legend, the reader is referred to the web version of this Letter.)

Table 1

Raw charge asymmetries for the $B^\pm \rightarrow \phi K^\pm$ and $B^\pm \rightarrow J/\psi K^\pm$ decays, their difference $\Delta\mathcal{A}_{CP}$, and the fraction of $B^\pm \rightarrow \phi K^\pm$ signal events in each trigger subsample for $k = \text{TOS, TIS}$. All uncertainties are statistical only.

	TOS subsample	TIS subsample
$\mathcal{A}_{\text{raw},k}(B^\pm \rightarrow \phi K^\pm)$	$+0.027 \pm 0.026$	-0.053 ± 0.035
$\mathcal{A}_{\text{raw},k}(B^\pm \rightarrow J/\psi K^\pm)$	-0.024 ± 0.008	-0.008 ± 0.005
$\Delta\mathcal{A}_{CP}$	$+0.052 \pm 0.027$	-0.045 ± 0.035
$N_k/(N_{\text{TOS}} + N_{\text{TIS}})$	66%	34%
Weighted $\Delta\mathcal{A}_{CP}$ average	$+0.019 \pm 0.021$	

Fig. 2 shows the projections of the fitting function superimposed on the m_{KKK} and m_{KK} distributions, shown separately for B^- and B^+ candidates, but where TOS and TIS events are summed. The m_{KKK} resolution measured from the fit is $\sigma_B = 20.4 \pm 0.3 \text{ MeV}/c^2$. The fitted raw asymmetries for the signal are shown in the first line of Table 1. They are statistically uncorrelated.

Each raw charge asymmetry is related to the CP asymmetry through

$$\mathcal{A}_{\text{raw},k}(B^\pm \rightarrow \phi K^\pm) = \mathcal{A}_{CP}(B^\pm \rightarrow \phi K^\pm) + \mathcal{A}_{D,k}(B^\pm \rightarrow \phi K^\pm) + \mathcal{A}_p, \quad (8)$$

where $\mathcal{A}_{D,k}(B^\pm \rightarrow \phi K^\pm)$ is the detection charge asymmetry for the bachelor K^\pm and \mathcal{A}_p is the production asymmetry of B^\pm

mesons. Eq. (8) and the corresponding equation for the $B^\pm \rightarrow J/\psi K^\pm$ reference channel hold because all involved asymmetries are small. Under the assumption that the detection asymmetry is the same for $B^\pm \rightarrow \phi K^\pm$ and $B^\pm \rightarrow J/\psi K^\pm$, which is correct in the limit where the bachelor K^\pm has the same kinematic properties, the difference in charge asymmetries defined in Eq. (2) can be written as

$$\Delta\mathcal{A}_{CP} = \mathcal{A}_{\text{raw},k}(B^\pm \rightarrow \phi K^\pm) - \mathcal{A}_{\text{raw},k}(B^\pm \rightarrow J/\psi K^\pm) \quad (9)$$

and should not depend on the trigger category k . The raw charge asymmetries of $B^\pm \rightarrow J/\psi K^\pm$ decays have been measured in a previous analysis [5]; they are subtracted from the $B^\pm \rightarrow \phi K^\pm$ raw asymmetries to obtain two independent measurements of $\Delta\mathcal{A}_{CP}$. Since the two results agree within about two statistical standard deviations, the results are combined. The final $\Delta\mathcal{A}_{CP}$ result is computed as a weighted average, with weights equal to the fractions $N_k/(N_{\text{TOS}} + N_{\text{TIS}})$ of signal events in the two trigger subsamples. All inputs to the calculation are reported in Table 1. The separation between TIS and TOS events is needed because the detection asymmetry $\mathcal{A}_{D,k}$ depends on the trigger category k and the fraction of events in the two categories differs between the signal and reference channels.

Several systematic uncertainties are considered on the weighted $\Delta\mathcal{A}_{CP}$ average, as summarized in Table 2. The contribution due to the mass shape modelling is obtained by repeating the fit (and the

Table 2
Systematic uncertainties on the measurement of $\Delta\mathcal{A}_{CP}$.

Source	Uncertainty
Mass shape modelling	0.003
Possible S-wave contribution	0.002
Trigger	0.004
Bachelor kaon kinematic properties	0.005
Geometric acceptance	0.002
Quadratic sum	0.007

calculation of Table 1) with the fixed parameter values of the Crystal Ball and ARGUS functions changed within their uncertainties, as determined from simulation and $B^\pm \rightarrow \phi K^\pm$ data, respectively, or with an exponential (rather than linear) combinatorial background model. Possible residual effects from S-wave contributions not fully accounted for by the linear component are investigated by comparing the observed angular distribution of the $B^\pm \rightarrow \phi K^\pm$ signal with the expectation for a peaking structure in the K^+K^- mass due to a single P-wave state. Other P-wave components are neglected. If these S-wave contributions corresponded to an additional component included in the signal without charge asymmetry, a bias would appear on $\Delta\mathcal{A}_{CP}$, which is taken as a systematic uncertainty.

The charge asymmetry in the trigger efficiency for kaons of the TOS subsample does not completely cancel in $\Delta\mathcal{A}_{CP}$, because of the different number of kaons in the two decay modes considered. The difference between the values of $\mathcal{A}_{\text{raw,TOS}}(B^\pm \rightarrow J/\psi K^\pm)$ computed with and without a charge-dependent correction for the kaon efficiency determined from calibration data is propagated as a systematic uncertainty on $\Delta\mathcal{A}_{CP}$. Such an effect is absent for the TIS subsample. Another small contribution, due to the TOS events that would still be accepted by the hardware trigger level without considering the particles from the B^+ candidate decay, has been included in the trigger systematic uncertainty. Due to differences in the kinematic selections of the $B^\pm \rightarrow \phi K^\pm$ and $B^\pm \rightarrow J/\psi K^\pm$ decay modes, the assumption of Eq. (9) cannot be exact, and a further systematic uncertainty is assigned. The fit of the raw charge asymmetries of $B^\pm \rightarrow J/\psi K^\pm$ is repeated with the same kinematic selection on the bachelor kaon as for $B^\pm \rightarrow \phi K^\pm$, i.e. $p > 10$ GeV/c and $p_T > 2.5$ GeV/c, and after reweighting its momentum distribution to that observed in the $B^\pm \rightarrow \phi K^\pm$ decays. The resulting effect on $\Delta\mathcal{A}_{CP}$ is taken as a systematic uncertainty. Finally, we repeat the $B^\pm \rightarrow \phi K^\pm$ analysis after requiring the bachelor kaon momentum to point in a fiducial solid angle avoiding detector edge effects, and assign the observed change in $\Delta\mathcal{A}_{CP}$ as a systematic uncertainty due to the geometrical acceptance.

The final measurement is

$$\Delta\mathcal{A}_{CP} = 0.019 \pm 0.021(\text{stat}) \pm 0.007(\text{syst}). \quad (10)$$

A recent update of the $B^\pm \rightarrow J/\psi K^\pm$ charge asymmetry measurement by the D0 Collaboration [20] has not been included yet in the average of the Particle Data Group (PDG) [1]. Replacing the previous D0 result with the new one yields the world average $\mathcal{A}_{CP}(B^\pm \rightarrow J/\psi K^\pm) = 0.003 \pm 0.006$, where the uncertainty is scaled by a factor 1.8 according to the PDG averaging rules. Using this average, we obtain

$$\mathcal{A}_{CP}(B^\pm \rightarrow \phi K^\pm) = 0.022 \pm 0.021(\text{stat}) \pm 0.009(\text{syst}), \quad (11)$$

where the uncertainty on the $B^\pm \rightarrow J/\psi K^\pm$ charge asymmetry is incorporated in the systematic uncertainty.

6. Search for $B^\pm \rightarrow \phi\pi^\pm$ decays

The search for $B^\pm \rightarrow \phi\pi^\pm$ decays is performed using a simultaneous fit to the $B^\pm \rightarrow \phi\pi^\pm$ ($\text{DLL}_{K\pi} < -1$) and $B^\pm \rightarrow \phi K^\pm$

($\text{DLL}_{K\pi} \geq -1$) candidates, dividing the $B^\pm \rightarrow \phi\pi^\pm$ candidates in four subsamples according to their δm values, each with its set of eight yields. The fit has a total of 52 free parameters: 15 mass shape parameters, 36 yields, and the ratio of the total $B^\pm \rightarrow \phi\pi^\pm$ yield to the total $B^\pm \rightarrow \phi K^\pm$ yield.

Fig. 3 shows the projections of the fitted function superimposed on the observed mass distributions of the $B^\pm \rightarrow \phi\pi^\pm$ candidates. The total $B^\pm \rightarrow \phi\pi^\pm$ signal yield is found to be 19 ± 19 , while the total $B^\pm \rightarrow \phi K^\pm$ yield is $(3486 \pm 76) + (280 \pm 25)$ summing the samples of $B^\pm \rightarrow \phi K^\pm$ and $B^\pm \rightarrow \phi\pi^\pm$ candidates. The fitted yield ratio is

$$\frac{N(B^\pm \rightarrow \phi\pi^\pm)}{N(B^\pm \rightarrow \phi K^\pm)} = (5.1_{-5.0}^{+5.3}(\text{stat}) \pm 2.1(\text{syst})) \times 10^{-3}, \quad (12)$$

where the systematic uncertainty is the quadratic sum of contributions due to the modelling of the mass shapes ($\pm 2.1 \times 10^{-3}$), the fit procedure ($\pm 0.2 \times 10^{-3}$), and interference effects between the ϕ resonance and a K^+K^- pair in an S-wave state ($\pm 0.4 \times 10^{-3}$). The first contribution is obtained by repeating the fit with the parameter values of the Crystal Ball and ARGUS functions changed within their uncertainties, or with an exponential (rather than linear) combinatorial background model. The dominant effect is due to the 8% uncertainty on the ratio ρ of the $B^\pm \rightarrow \phi K^\pm$ mass resolutions in the two $\text{DLL}_{K\pi}$ regions. Simulation studies show that the fit procedure is unbiased, and the statistical precision of this check is assigned as a systematic uncertainty.

The measurement of the branching fraction ratio is obtained as the ratio between Eq. (12) and Eq. (3):

$$\frac{\mathcal{B}(B^\pm \rightarrow \phi\pi^\pm)}{\mathcal{B}(B^\pm \rightarrow \phi K^\pm)} = (6.6_{-6.6}^{+6.9}(\text{stat}) \pm 2.8(\text{syst})) \times 10^{-3}. \quad (13)$$

Since the result is not significantly different from zero, we also quote upper limits from the integral of the likelihood function of this ratio, considering only the physical (non-negative) region. Including systematic uncertainties we obtain $\mathcal{B}(B^\pm \rightarrow \phi\pi^\pm)/\mathcal{B}(B^\pm \rightarrow \phi K^\pm) < 0.018(0.020)$ at 90% (95%) CL. Using the current world average $\mathcal{B}(B^\pm \rightarrow \phi K^\pm) = (8.8_{-0.6}^{+0.7}) \times 10^{-6}$ [1], we finally obtain

$$\mathcal{B}(B^\pm \rightarrow \phi\pi^\pm) = (5.8_{-5.8}^{+6.1} \pm 2.5) \times 10^{-8} \quad (14)$$

$$< 1.5(1.8) \times 10^{-7} \quad \text{at 90\% (95\%) CL.} \quad (15)$$

7. Conclusions

The difference in charge asymmetries between the $B^\pm \rightarrow \phi K^\pm$ and $B^\pm \rightarrow J/\psi K^\pm$ decay modes is measured in a sample of pp collisions at 7 TeV centre-of-mass energy, corresponding to an integrated luminosity of 1.0 fb^{-1} collected with the LHCb detector. Using the known value of the $B^\pm \rightarrow J/\psi K^\pm$ asymmetry, the CP -violating charge asymmetry of $B^\pm \rightarrow \phi K^\pm$ decays is determined to be $\mathcal{A}_{CP}(B^\pm \rightarrow \phi K^\pm) = 0.022 \pm 0.021(\text{stat}) \pm 0.009(\text{syst})$. This result is almost a factor two more precise than the current world average [1]. It is consistent with both the absence of CP violation and the Standard Model prediction.

A search for $B^\pm \rightarrow \phi\pi^\pm$ decays is also performed. No significant signal is found. Using the known branching fraction of the $B^\pm \rightarrow \phi K^\pm$ normalization channel, an upper limit of $\mathcal{B}(B^\pm \rightarrow \phi\pi^\pm) < 1.5(1.8) \times 10^{-7}$ is set at 90% (95%) confidence level. This improves on the previous best upper limit [19], while reaching the upper end of the Standard Model predictions.

Acknowledgements

We express our gratitude to our colleagues in the CERN accelerator departments for the excellent performance of the LHC.

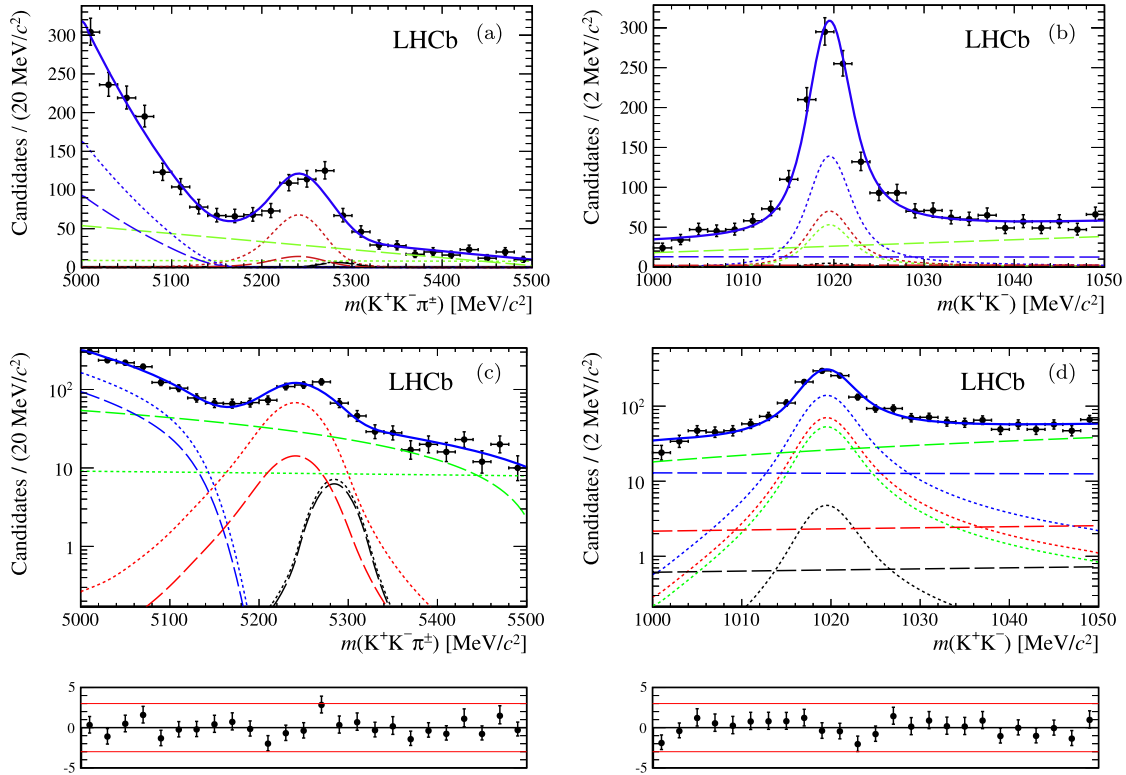


Fig. 3. Distributions of the (a, c) $K^+K^-\pi^\pm$ and (b, d) K^+K^- masses of the selected $B^\pm \rightarrow \phi\pi^\pm$ candidates, shown both with linear and logarithmic scales. The solid blue curves represent the result of the simultaneous fit described in the text, with the following components: $B^\pm \rightarrow \phi\pi^\pm$ signal (dotted black), nonresonant $B^\pm \rightarrow K^+K^-\pi^\pm$ background (dashed black), $B^\pm \rightarrow \phi K^\pm$ signal (dotted red), nonresonant $B^\pm \rightarrow K^+K^-K^\pm$ background (dashed red), partially-reconstructed b -hadron background with (dotted blue) or without (dashed blue) a true ϕ meson, and combinatorial background with (dotted green) or without (dashed green) a true ϕ meson. Normalized residuals are displayed below the histograms. (For interpretation of the references to colour in this figure legend, the reader is referred to the web version of this Letter.)

We thank the technical and administrative staff at the LHCb institutes. We acknowledge support from CERN and from the national agencies: CAPES, CNPq, FAPERJ and FINEP (Brazil); NSFC (China); CNRS/IN2P3 and Region Auvergne (France); BMBF, DFG, HGF and MPG (Germany); SFI (Ireland); INFN (Italy); FOM and NWO (The Netherlands); SCSR (Poland); MEN/IFA (Romania); MinES, Rosatom, RFBR and NRC “Kurchatov Institute” (Russia); MinEco, XuntaGal and GENCAT (Spain); SNSF and SER (Switzerland); NAS Ukraine (Ukraine); STFC (United Kingdom); NSF (USA). We also acknowledge the support received from the ERC under FP7. The Tier1 computing centres are supported by IN2P3 (France), KIT and BMBF (Germany), INFN (Italy), NWO and SURF (The Netherlands), PIC (Spain), GridPP (United Kingdom). We are thankful for the computing resources put at our disposal by Yandex LLC (Russia), as well as to the communities behind the multiple open source software packages that we depend on.

References

- [1] Particle Data Group, J. Beringer, et al., Review of particle physics, *Phys. Rev. D* 86 (2012) 010001, and 2013 partial update for the 2014 edition.
- [2] H.-n. Li, S. Mishima, Penguin-dominated $B \rightarrow PV$ decays in NLO perturbative QCD, *Phys. Rev. D* 74 (2006) 094020, arXiv:hep-ph/0608277.
- [3] M. Beneke, M. Neubert, QCD factorization for $B \rightarrow PP$ and $B \rightarrow PV$ decays, *Nucl. Phys. B* 675 (2003) 333, arXiv:hep-ph/0308039.
- [4] BaBar Collaboration, J.P. Lees, et al., Study of CP violation in Dalitz-plot analyses of $B^0 \rightarrow K^+K^-K_S^0$, $B^+ \rightarrow K^+K^-K^+$, and $B^+ \rightarrow K_S^0K_S^0K^+$, *Phys. Rev. D* 85 (2012) 112010, arXiv:1201.5897.
- [5] LHCb Collaboration, R. Aaij, et al., Measurement of CP violation in the phase space of $B^\pm \rightarrow K^\pm\pi^+\pi^-$ and $B^\pm \rightarrow K^\pm K^+K^-$, *Phys. Rev. Lett.* 111 (2013) 101801, arXiv:1306.1246.
- [6] N. Cabibbo, Unitary symmetry and leptonic decays, *Phys. Rev. Lett.* 10 (1963) 531.
- [7] M. Kobayashi, T. Maskawa, CP violation in the renormalizable theory of weak interaction, *Prog. Theor. Phys.* 49 (1973) 652.
- [8] S. Okubo, ϕ -meson and unitary symmetry model, *Phys. Lett.* 5 (1963) 165.
- [9] G. Zweig, An SU_3 model for strong interaction symmetry and its breaking, CERN-TH-401 and CERN-TH-412, 1964.
- [10] J. Iizuka, A systematics and phenomenology of meson family, *Prog. Theor. Phys. Suppl.* 37–38 (1966) 21.
- [11] S. Bar-Shalom, G. Eilam, Y.-D. Yang, $B \rightarrow \phi\pi$ and $B^0 \rightarrow \phi\phi$ in the Standard Model and new bounds on R parity violation, *Phys. Rev. D* 67 (2003) 014007, arXiv:hep-ph/0201244.
- [12] Y. Li, C.-D. Lu, W. Wang, Revisiting $B \rightarrow \phi\pi$ decays in the Standard Model, *Phys. Rev. D* 80 (2009) 014024, arXiv:0901.0648.
- [13] A. Kucukarslan, U.-G. Meissner, ω - ϕ mixing in chiral perturbation theory, *Mod. Phys. Lett. A* 21 (2006) 1423, arXiv:hep-ph/0603061.
- [14] M. Benayoun, et al., Radiative decays, nonet symmetry and $SU(3)$ breaking, *Phys. Rev. D* 59 (1999) 114027, arXiv:hep-ph/9902326.
- [15] M. Benayoun, et al., The dipion mass spectrum in e^+e^- annihilation and τ decay: a dynamical (ρ , ω , ϕ) mixing approach, *Eur. Phys. J. C* 55 (2008) 199, arXiv:0711.4482.
- [16] M. Benayoun, P. David, L. DelBuono, O. Leitner, A global treatment of VMD physics up to the ϕ : I. e^+e^- annihilations, anomalies and vector meson partial widths, *Eur. Phys. J. C* 65 (2010) 211, arXiv:0907.4047.
- [17] M. Gronau, J.L. Rosner, B decays dominated by ω - ϕ mixing, *Phys. Lett. B* 666 (2008) 185, arXiv:0806.3584.
- [18] LHCb Collaboration, R. Aaij, et al., First observation of $B^0 \rightarrow J/\psi K^+K^-$ and search for $B^0 \rightarrow J/\psi\phi$ decays, arXiv:1308.5916.
- [19] BaBar Collaboration, B. Aubert, et al., Search for $B^+ \rightarrow \phi\pi^+$ and $B^0 \rightarrow \phi\pi^0$ decays, *Phys. Rev. D* 74 (2006) 011102, arXiv:hep-ex/0605037.
- [20] D0 Collaboration, V.M. Abazov, et al., Measurement of direct CP violation parameters in $B^\pm \rightarrow J/\psi K^\pm$ and $B^\pm \rightarrow J/\psi\pi^\pm$ decays with 10.4 fb^{-1} of Tevatron data, *Phys. Rev. Lett.* 110 (2013) 241801, arXiv:1304.1655.
- [21] LHCb Collaboration, A.A. Alves Jr., et al., The LHCb detector at the LHC, *J. Instrum.* 3 (2008) S08005.
- [22] M. Adinolfi, et al., Performance of the LHCb RICH detector at the LHC, *Eur. Phys. J. C* 73 (2013) 2431, arXiv:1211.6759.

- [23] R. Aaij, et al., The LHCb trigger and its performance in 2011, *J. Instrum.* 8 (2013) P04022, arXiv:1211.3055.
- [24] V.V. Gligorov, M. Williams, Efficient, reliable and fast high-level triggering using a bonsai boosted decision tree, *J. Instrum.* 8 (2013) P02013, arXiv:1210.6861.
- [25] T. Sjöstrand, S. Mrenna, P. Skands, PYTHIA 6.4 physics and manual, *J. High Energy Phys.* 0605 (2006) 026, arXiv:hep-ph/0603175.
- [26] I. Belyaev, et al., Handling of the generation of primary events in Gauss, the LHCb simulation framework, *IEEE Nucl. Sci. Symp. Conf. Rec.* (2010) 1155.
- [27] D.J. Lange, The EvtGen particle decay simulation package, *Nucl. Instrum. Methods* 462 (2001) 152.
- [28] P. Golonka, Z. Was, PHOTOS Monte Carlo: a precision tool for QED corrections in Z and W decays, *Eur. Phys. J. C* 45 (2006) 97, arXiv:hep-ph/0506026.
- [29] Geant4 Collaboration, J. Allison, et al., Geant4 developments and applications, *IEEE Trans. Nucl. Sci.* 53 (2006) 270; Geant4 Collaboration, S. Agostinelli, et al., Geant4: a simulation toolkit, *Nucl. Instrum. Methods* 506 (2003) 250.
- [30] M. Clemencic, et al., The LHCb simulation application, Gauss: design, evolution and experience, *J. Phys. Conf. Ser.* 331 (2011) 032023.
- [31] T. Skwarnicki, A study of the radiative cascade transitions between the Upsilon-prime and Upsilon resonances, PhD thesis, Institute of Nuclear Physics, Krakow, 1986, DESY-F31-86-02.
- [32] ARGUS Collaboration, H. Albrecht, et al., Search for $b \rightarrow s\gamma$ in exclusive decays of B mesons, *Phys. Lett. B* 229 (1989) 304.
- [33] G. Punzi, Comments on likelihood fits with variable resolution, eConf C 030908 (2003) WELT002, arXiv:physics/0401045.

LHCb Collaboration

R. Aaij⁴⁰, B. Adeva³⁶, M. Adinolfi⁴⁵, C. Adrover⁶, A. Affolder⁵¹, Z. Ajaltouni⁵, J. Albrecht⁹, F. Alessio³⁷, M. Alexander⁵⁰, S. Ali⁴⁰, G. Alkhazov²⁹, P. Alvarez Cartelle³⁶, A.A. Alves Jr.²⁴, S. Amato², S. Amerio²¹, Y. Amhis⁷, L. Anderlini^{17,f}, J. Anderson³⁹, R. Andreassen⁵⁶, J.E. Andrews⁵⁷, R.B. Appleby⁵³, O. Aquines Gutierrez¹⁰, F. Archilli¹⁸, A. Artamonov³⁴, M. Artuso⁵⁸, E. Aslanides⁶, G. Auremma^{24,m}, M. Baalouch⁵, S. Bachmann¹¹, J.J. Back⁴⁷, A. Badalov³⁵, C. Baesso^{59,t}, V. Balagura³⁰, W. Baldini¹⁶, R.J. Barlow⁵³, C. Barschel³⁷, S. Barsuk⁷, W. Barter⁴⁶, Th. Bauer⁴⁰, A. Bay³⁸, J. Beddow⁵⁰, F. Bedeschi²², I. Bediaga¹, S. Belogurov³⁰, K. Belous³⁴, I. Belyaev³⁰, E. Ben-Haim⁸, G. Bencivenni¹⁸, S. Benson⁴⁹, J. Benton⁴⁵, A. Berezhnoy³¹, R. Bernet³⁹, M.-O. Bettler⁴⁶, M. van Beuzekom⁴⁰, A. Bien¹¹, S. Bifani⁴⁴, T. Bird⁵³, A. Bizzeti^{17,h}, P.M. Bjørnstad⁵³, T. Blake³⁷, F. Blanc³⁸, J. Blouw¹⁰, S. Blusk⁵⁸, V. Bocci²⁴, A. Bondar³³, N. Bondar²⁹, W. Bonivento¹⁵, S. Borghi⁵³, A. Borgia⁵⁸, T.J.V. Bowcock⁵¹, E. Bowen³⁹, C. Bozzi¹⁶, T. Brambach⁹, J. van den Brand⁴¹, J. Bressieux³⁸, D. Brett⁵³, M. Britsch¹⁰, T. Britton⁵⁸, N.H. Brook⁴⁵, H. Brown⁵¹, A. Bursche³⁹, G. Busetto^{21,q}, J. Buytaert³⁷, S. Cadeddu¹⁵, O. Callot⁷, M. Calvi^{20,j}, M. Calvo Gomez^{35,n}, A. Camboni³⁵, P. Campana^{18,37}, D. Campora Perez³⁷, A. Carbone^{14,c}, G. Carboni^{23,k}, R. Cardinale^{19,i}, A. Cardini¹⁵, H. Carranza-Mejia⁴⁹, L. Carson⁵², K. Carvalho Akiba², G. Casse⁵¹, L. Castillo Garcia³⁷, M. Cattaneo³⁷, Ch. Cauet⁹, R. Cenci⁵⁷, M. Charles⁵⁴, Ph. Charpentier³⁷, P. Chen^{3,38}, S.-F. Cheung⁵⁴, N. Chiapolini³⁹, M. Chrzaszcz^{39,25}, K. Ciba³⁷, X. Cid Vidal³⁷, G. Ciezarek⁵², P.E.L. Clarke⁴⁹, M. Clemencic³⁷, H.V. Cliff⁴⁶, J. Closier³⁷, C. Coca²⁸, V. Coco⁴⁰, J. Cogan⁶, E. Cogneras⁵, P. Collins³⁷, A. Comerma-Montells³⁵, A. Contu^{15,37}, A. Cook⁴⁵, M. Coombes⁴⁵, S. Coquereau⁸, G. Corti³⁷, B. Couturier³⁷, G.A. Cowan⁴⁹, D.C. Craik⁴⁷, M. Cruz Torres^{59,t}, S. Cunliffe⁵², R. Currie⁴⁹, C. D'Ambrosio³⁷, P. David⁸, P.N.Y. David⁴⁰, A. Davis⁵⁶, I. De Bonis⁴, K. De Bruyn⁴⁰, S. De Capua⁵³, M. De Cian¹¹, J.M. De Miranda¹, L. De Paula², W. De Silva⁵⁶, P. De Simone¹⁸, D. Decamp⁴, M. Deckenhoff⁹, L. Del Buono⁸, N. Déleage⁴, D. Derkach⁵⁴, O. Deschamps⁵, F. Dettori⁴¹, A. Di Canto¹¹, H. Dijkstra³⁷, M. Dogaru²⁸, S. Donleavy⁵¹, F. Dordei¹¹, A. Dosil Suárez³⁶, D. Dossett⁴⁷, A. Dovbnya⁴², F. Dupertuis³⁸, P. Durante³⁷, R. Dzhelyadin³⁴, A. Dziurda²⁵, A. Dzyuba²⁹, S. Easo⁴⁸, U. Egede⁵², V. Egorychev³⁰, S. Eidelman³³, D. van Eijk⁴⁰, S. Eisenhardt⁴⁹, U. Eitschberger⁹, R. Ekelhof⁹, L. Eklund^{50,37}, I. El Rifai⁵, Ch. Elsasser³⁹, A. Falabella^{14,e}, C. Färber¹¹, C. Farinelli⁴⁰, S. Farry⁵¹, D. Ferguson⁴⁹, V. Fernandez Albor³⁶, F. Ferreira Rodrigues¹, M. Ferro-Luzzi³⁷, S. Filippov³², M. Fiore^{16,e}, C. Fitzpatrick³⁷, M. Fontana¹⁰, F. Fontanelli^{19,i}, R. Forty³⁷, O. Francisco², M. Frank³⁷, C. Frei³⁷, M. Frosini^{17,37,f}, E. Furfaro^{23,k}, A. Gallas Torreira³⁶, D. Galli^{14,c}, M. Gandelman², P. Gandini⁵⁸, Y. Gao³, J. Garofoli⁵⁸, P. Garosi⁵³, J. Garra Tico⁴⁶, L. Garrido³⁵, C. Gaspar³⁷, R. Gauld⁵⁴, E. Gersabeck¹¹, M. Gersabeck⁵³, T. Gershon⁴⁷, Ph. Ghez⁴, V. Gibson⁴⁶, L. Giubega²⁸, V.V. Gligorov³⁷, C. Göbel^{59,t}, D. Golubkov³⁰, A. Golutvin^{52,30,37}, A. Gomes², P. Gorbounov^{30,37}, H. Gordon³⁷, M. Grabalosa Gándara⁵, R. Graciani Diaz³⁵, L.A. Granado Cardoso³⁷, E. Graugés³⁵, G. Graziani¹⁷, A. Grecu²⁸, E. Greening⁵⁴, S. Gregson⁴⁶, P. Griffith⁴⁴, O. Grünberg^{60,u}, B. Gui⁵⁸, E. Gushchin³², Yu. Guz^{34,37}, T. Gys³⁷, C. Hadjivasiliou⁵⁸, G. Haefeli³⁸, C. Haen³⁷, S.C. Haines⁴⁶, S. Hall⁵², B. Hamilton⁵⁷, T. Hampson⁴⁵, S. Hansmann-Menzemer¹¹, N. Harnew⁵⁴, S.T. Harnew⁴⁵, J. Harrison⁵³, T. Hartmann^{60,u}, J. He³⁷, T. Head³⁷, V. Heijne⁴⁰, K. Hennessy⁵¹, P. Henrard⁵, J.A. Hernando Morata³⁶, E. van Herwijnen³⁷, M. Heß^{60,u}, A. Hicheur¹, E. Hicks⁵¹, D. Hill⁵⁴, M. Hoballah⁵, C. Hombach⁵³, W. Hulsbergen⁴⁰, P. Hunt⁵⁴, T. Huse⁵¹, N. Hussain⁵⁴, D. Hutchcroft⁵¹, D. Hynds⁵⁰, V. Iakovenko⁴³, M. Idzik²⁶, P. Ilten¹², R. Jacobsson³⁷, A. Jaeger¹¹, E. Jans⁴⁰, P. Jaton³⁸, A. Jawahery⁵⁷, F. Jing³, M. John⁵⁴, D. Johnson⁵⁴,

C.R. Jones⁴⁶, C. Joram³⁷, B. Jost³⁷, M. Kabbalo⁹, S. Kandybei⁴², W. Kanso⁶, M. Karacson³⁷, T.M. Karbach³⁷, I.R. Kenyon⁴⁴, T. Ketel⁴¹, B. Khanji²⁰, O. Kochebina⁷, I. Komarov³⁸, R.F. Koopman⁴¹, P. Koppenburg⁴⁰, M. Korolev³¹, A. Kozlinskiy⁴⁰, L. Kravchuk³², K. Kreplin¹¹, M. Kreps⁴⁷, G. Krocker¹¹, P. Krokovny³³, F. Kruse⁹, M. Kucharczyk^{20,25,37,j}, V. Kudryavtsev³³, K. Kurek²⁷, T. Kvaratskheliya^{30,37}, V.N. La Thi³⁸, D. Lacarrere³⁷, G. Lafferty⁵³, A. Lai¹⁵, D. Lambert⁴⁹, R.W. Lambert⁴¹, E. Lanciotti³⁷, G. Lanfranchi¹⁸, C. Langenbruch³⁷, T. Latham⁴⁷, C. Lazzeroni⁴⁴, R. Le Gac⁶, J. van Leerdam⁴⁰, J.-P. Lees⁴, R. Lefèvre⁵, A. Leflat³¹, J. Lefrançois⁷, S. Leo²², O. Leroy⁶, T. Lesiak²⁵, B. Leverington¹¹, Y. Li³, L. Li Gioi⁵, M. Liles⁵¹, R. Lindner³⁷, C. Linn¹¹, B. Liu³, G. Liu³⁷, S. Lohn³⁷, I. Longstaff⁵⁰, J.H. Lopes², N. Lopez-March³⁸, H. Lu³, D. Lucchesi^{21,q}, J. Luisier³⁸, H. Luo⁴⁹, O. Lupton⁵⁴, F. Machefert⁷, I.V. Machikhiliyan³⁰, F. Maciuc²⁸, O. Maev^{29,37}, S. Malde⁵⁴, G. Manca^{15,d}, G. Mancinelli⁶, J. Maratas⁵, U. Marconi¹⁴, P. Marino^{22,s}, R. Märki³⁸, J. Marks¹¹, G. Martellotti²⁴, A. Martens⁸, A. Martín Sánchez⁷, M. Martinelli⁴⁰, D. Martinez Santos^{41,37}, D. Martins Tostes², A. Martynov³¹, A. Massafferri¹, R. Matev³⁷, Z. Mathe³⁷, C. Matteuzzi²⁰, E. Maurice⁶, A. Mazurov^{16,37,e}, J. McCarthy⁴⁴, A. McNab⁵³, R. McNulty¹², B. McSkelly⁵¹, B. Meadows^{56,54}, F. Meier⁹, M. Meissner¹¹, M. Merk⁴⁰, D.A. Milanes⁸, M.-N. Minard⁴, J. Molina Rodriguez^{59,t}, S. Monteil⁵, D. Moran⁵³, P. Morawski²⁵, A. Mordà⁶, M.J. Morello^{22,s}, R. Mountain⁵⁸, I. Mous⁴⁰, F. Muheim⁴⁹, K. Müller³⁹, R. Muresan²⁸, B. Muryn²⁶, B. Muster³⁸, P. Naik⁴⁵, T. Nakada³⁸, R. Nandakumar⁴⁸, I. Nasteva¹, M. Needham⁴⁹, S. Neubert³⁷, N. Neufeld³⁷, A.D. Nguyen³⁸, T.D. Nguyen³⁸, C. Nguyen-Mau^{38,o}, M. Nicol⁷, V. Niess⁵, R. Niet⁹, N. Nikitin³¹, T. Nikodem¹¹, A. Nomerotski⁵⁴, A. Novoselov³⁴, A. Oblakowska-Mucha²⁶, V. Obraztsov³⁴, S. Oggero⁴⁰, S. Ogilvy⁵⁰, O. Okhrimenko⁴³, R. Oldeman^{15,d}, M. Orlandea²⁸, J.M. Otalora Goicochea², P. Owen⁵², A. Oyanguren³⁵, B.K. Pal⁵⁸, A. Palano^{13,b}, M. Palutan¹⁸, J. Panman³⁷, A. Papanestis⁴⁸, M. Pappagallo⁵⁰, C. Parkes⁵³, C.J. Parkinson⁵², G. Passaleva¹⁷, G.D. Patel⁵¹, M. Patel⁵², G.N. Patrick⁴⁸, C. Patrignani^{19,i}, C. Pavel-Nicorescu²⁸, A. Pazos Alvarez³⁶, A. Pearce⁵³, A. Pellegrino⁴⁰, G. Penso^{24,l}, M. Pepe Altarelli³⁷, S. Perazzini^{14,c}, E. Perez Trigo³⁶, A. Pérez-Calero Yzquierdo³⁵, P. Perret⁵, M. Perrin-Terrin⁶, L. Pescatore⁴⁴, E. Pesen^{61,v}, G. Pessina²⁰, K. Petridis⁵², A. Petrolini^{19,i}, A. Phan⁵⁸, E. Picatoste Olloqui³⁵, B. Pietrzyk⁴, T. Pilař⁴⁷, D. Pinci²⁴, S. Playfer⁴⁹, M. Plo Casasus³⁶, F. Polci⁸, G. Polok²⁵, A. Poluektov^{47,33}, E. Polcarpo², A. Popov³⁴, D. Popov¹⁰, B. Popovici²⁸, C. Potterat³⁵, A. Powell⁵⁴, J. Prisciandaro^{38,*}, A. Pritchard⁵¹, C. Prouve⁷, V. Pugatch⁴³, A. Puig Navarro³⁸, G. Punzi^{22,r}, W. Qian⁴, B. Rachwal²⁵, J.H. Rademacker⁴⁵, B. Rakotomiaramanana³⁸, M.S. Rangel², I. Raniuk⁴², N. Rauschmayr³⁷, G. Raven⁴¹, S. Redford⁵⁴, S. Reichert⁵³, M.M. Reid⁴⁷, A.C. dos Reis¹, S. Ricciardi⁴⁸, A. Richards⁵², K. Rinnert⁵¹, V. Rives Molina³⁵, D.A. Roa Romero⁵, P. Robbe⁷, D.A. Roberts⁵⁷, A.B. Rodrigues¹, E. Rodrigues⁵³, P. Rodriguez Perez³⁶, S. Roiser³⁷, V. Romanovsky³⁴, A. Romero Vidal³⁶, J. Rouvinet³⁸, T. Ruf³⁷, F. Ruffini²², H. Ruiz³⁵, P. Ruiz Valls³⁵, G. Sabatino^{24,k}, J.J. Saborido Silva³⁶, N. Sagidova²⁹, P. Sail⁵⁰, B. Saitta^{15,d}, V. Salustino Guimaraes², B. Sanmartin Sedes³⁶, R. Santacesaria²⁴, C. Santamarina Rios³⁶, E. Santovetti^{23,k}, M. Sapunov⁶, A. Sarti¹⁸, C. Satriano^{24,m}, A. Satta²³, M. Savrie^{16,e}, D. Savrina^{30,31}, M. Schiller⁴¹, H. Schindler³⁷, M. Schlupp⁹, M. Schmelling¹⁰, B. Schmidt³⁷, O. Schneider³⁸, A. Schopper³⁷, M.-H. Schune⁷, R. Schwemmer³⁷, B. Sciascia¹⁸, A. Sciubba²⁴, M. Seco³⁶, A. Semennikov³⁰, K. Senderowska²⁶, I. Sepp⁵², N. Serra³⁹, J. Serrano⁶, P. Seyfert¹¹, M. Shapkin³⁴, I. Shapoval^{16,42,e}, Y. Shcheglov²⁹, T. Shears⁵¹, L. Shekhtman³³, O. Shevchenko⁴², V. Shevchenko³⁰, A. Shires⁹, R. Silva Coutinho⁴⁷, M. Sirendi⁴⁶, N. Skidmore⁴⁵, T. Skwarnicki⁵⁸, N.A. Smith⁵¹, E. Smith^{54,48}, E. Smith⁵², J. Smith⁴⁶, M. Smith⁵³, M.D. Sokoloff⁵⁶, F.J.P. Soler⁵⁰, F. Soomro³⁸, D. Souza⁴⁵, B. Souza De Paula², B. Spaan⁹, A. Sparkes⁴⁹, P. Spradlin⁵⁰, F. Stagni³⁷, S. Stahl¹¹, O. Steinkamp³⁹, S. Stevenson⁵⁴, S. Stoica²⁸, S. Stone⁵⁸, B. Storaci³⁹, M. Straticicuc²⁸, U. Straumann³⁹, V.K. Subbiah³⁷, L. Sun⁵⁶, W. Sutcliffe⁵², S. Swientek⁹, V. Syropoulos⁴¹, M. Szczekowski²⁷, P. Szczypka^{38,37}, D. Szilard², T. Szumlak²⁶, S. T'Jampens⁴, M. Teklishyn⁷, E. Teodorescu²⁸, F. Teubert³⁷, C. Thomas⁵⁴, E. Thomas³⁷, J. van Tilburg¹¹, V. Tisserand⁴, M. Tobin³⁸, S. Tolki⁴¹, D. Tonelli³⁷, S. Topp-Joergensen⁵⁴, N. Torr⁵⁴, E. Tournefier^{4,52}, S. Tourneur³⁸, M.T. Tran³⁸, M. Tresch³⁹, A. Tsaregorodtsev⁶, P. Tsopelas⁴⁰, N. Tuning^{40,37}, M. Ubeda Garcia³⁷, A. Ukleja²⁷, A. Ustyuzhanin^{52,p}, U. Uwer¹¹, V. Vagnoni¹⁴, G. Valenti¹⁴, A. Vallier⁷, R. Vazquez Gomez¹⁸, P. Vazquez Regueiro³⁶, C. Vázquez Sierra³⁶, S. Vecchi¹⁶, J.J. Velthuis⁴⁵, M. Veltri^{17,g}, G. Veneziano³⁸, M. Vesterinen³⁷, B. Viaud⁷, D. Vieira², X. Vilasis-Cardona^{35,n}, A. Vollhardt³⁹, D. Volynskyy¹⁰, D. Voong⁴⁵, A. Vorobyev²⁹, V. Vorobyev³³, C. Voß^{60,u}, H. Voss¹⁰, R. Waldi^{60,u}, C. Wallace⁴⁷,

R. Wallace¹², S. Wandernoth¹¹, J. Wang⁵⁸, D.R. Ward⁴⁶, N.K. Watson⁴⁴, A.D. Webber⁵³, D. Websdale⁵², M. Whitehead⁴⁷, J. Wicht³⁷, J. Wiechczynski²⁵, D. Wiedner¹¹, L. Wiggers⁴⁰, G. Wilkinson⁵⁴, M.P. Williams^{47,48}, M. Williams⁵⁵, F.F. Wilson⁴⁸, J. Wimberley⁵⁷, J. Wishahi⁹, W. Wislicki²⁷, M. Witek²⁵, G. Wormser⁷, S.A. Wotton⁴⁶, S. Wright⁴⁶, S. Wu³, K. Wyllie³⁷, Y. Xie^{49,37}, Z. Xing⁵⁸, Z. Yang³, X. Yuan³, O. Yushchenko³⁴, M. Zangoli¹⁴, M. Zavertyaev^{10,a}, F. Zhang³, L. Zhang⁵⁸, W.C. Zhang¹², Y. Zhang³, A. Zhelezov¹¹, A. Zhokhov³⁰, L. Zhong³, A. Zvyagin³⁷

¹ Centro Brasileiro de Pesquisas Físicas (CBPF), Rio de Janeiro, Brazil

² Universidade Federal do Rio de Janeiro (UFRJ), Rio de Janeiro, Brazil

³ Center for High Energy Physics, Tsinghua University, Beijing, China

⁴ LAPP, Université de Savoie, CNRS/IN2P3, Annecy-Le-Vieux, France

⁵ Clermont Université, Université Blaise Pascal, CNRS/IN2P3, LPC, Clermont-Ferrand, France

⁶ CPPM, Aix-Marseille Université, CNRS/IN2P3, Marseille, France

⁷ LAL, Université Paris-Sud, CNRS/IN2P3, Orsay, France

⁸ LPNHE, Université Pierre et Marie Curie, Université Paris Diderot, CNRS/IN2P3, Paris, France

⁹ Fakultät Physik, Technische Universität Dortmund, Dortmund, Germany

¹⁰ Max-Planck-Institut für Kernphysik (MPIK), Heidelberg, Germany

¹¹ Physikalisches Institut, Ruprecht-Karls-Universität Heidelberg, Heidelberg, Germany

¹² School of Physics, University College Dublin, Dublin, Ireland

¹³ Sezione INFN di Bari, Bari, Italy

¹⁴ Sezione INFN di Bologna, Bologna, Italy

¹⁵ Sezione INFN di Cagliari, Cagliari, Italy

¹⁶ Sezione INFN di Ferrara, Ferrara, Italy

¹⁷ Sezione INFN di Firenze, Firenze, Italy

¹⁸ Laboratori Nazionali dell'INFN di Frascati, Frascati, Italy

¹⁹ Sezione INFN di Genova, Genova, Italy

²⁰ Sezione INFN di Milano Bicocca, Milano, Italy

²¹ Sezione INFN di Padova, Padova, Italy

²² Sezione INFN di Pisa, Pisa, Italy

²³ Sezione INFN di Roma Tor Vergata, Roma, Italy

²⁴ Sezione INFN di Roma La Sapienza, Roma, Italy

²⁵ Henryk Niewodniczanski Institute of Nuclear Physics, Polish Academy of Sciences, Kraków, Poland

²⁶ AGH – University of Science and Technology, Faculty of Physics and Applied Computer Science, Kraków, Poland

²⁷ National Center for Nuclear Research (NCBJ), Warsaw, Poland

²⁸ Horia Hulubei National Institute of Physics and Nuclear Engineering, Bucharest-Magurele, Romania

²⁹ Petersburg Nuclear Physics Institute (PNPI), Gatchina, Russia

³⁰ Institute of Theoretical and Experimental Physics (ITEP), Moscow, Russia

³¹ Institute of Nuclear Physics, Moscow State University (SINP MSU), Moscow, Russia

³² Institute for Nuclear Research of the Russian Academy of Sciences (INR RAN), Moscow, Russia

³³ Budker Institute of Nuclear Physics (SB RAS) and Novosibirsk State University, Novosibirsk, Russia

³⁴ Institute for High Energy Physics (IHEP), Protvino, Russia

³⁵ Universitat de Barcelona, Barcelona, Spain

³⁶ Universidad de Santiago de Compostela, Santiago de Compostela, Spain

³⁷ European Organization for Nuclear Research (CERN), Geneva, Switzerland

³⁸ Ecole Polytechnique Fédérale de Lausanne (EPFL), Lausanne, Switzerland

³⁹ Physik-Institut, Universität Zürich, Zürich, Switzerland

⁴⁰ Nikhef National Institute for Subatomic Physics, Amsterdam, The Netherlands

⁴¹ Nikhef National Institute for Subatomic Physics and VU University Amsterdam, Amsterdam, The Netherlands

⁴² NSC Kharkiv Institute of Physics and Technology (NSC KIPT), Kharkiv, Ukraine

⁴³ Institute for Nuclear Research of the National Academy of Sciences (KINR), Kyiv, Ukraine

⁴⁴ University of Birmingham, Birmingham, United Kingdom

⁴⁵ H.H. Wills Physics Laboratory, University of Bristol, Bristol, United Kingdom

⁴⁶ Cavendish Laboratory, University of Cambridge, Cambridge, United Kingdom

⁴⁷ Department of Physics, University of Warwick, Coventry, United Kingdom

⁴⁸ STFC Rutherford Appleton Laboratory, Didcot, United Kingdom

⁴⁹ School of Physics and Astronomy, University of Edinburgh, Edinburgh, United Kingdom

⁵⁰ School of Physics and Astronomy, University of Glasgow, Glasgow, United Kingdom

⁵¹ Oliver Lodge Laboratory, University of Liverpool, Liverpool, United Kingdom

⁵² Imperial College London, London, United Kingdom

⁵³ School of Physics and Astronomy, University of Manchester, Manchester, United Kingdom

⁵⁴ Department of Physics, University of Oxford, Oxford, United Kingdom

⁵⁵ Massachusetts Institute of Technology, Cambridge, MA, United States

⁵⁶ University of Cincinnati, Cincinnati, OH, United States

⁵⁷ University of Maryland, College Park, MD, United States

⁵⁸ Syracuse University, Syracuse, NY, United States

⁵⁹ Pontifícia Universidade Católica do Rio de Janeiro (PUC-Rio), Rio de Janeiro, Brazil[†]

⁶⁰ Institut für Physik, Universität Rostock, Rostock, Germany[‡]

⁶¹ Celal Bayar University, Manisa, Turkey[‡]

* Corresponding author.

^a P.N. Lebedev Physical Institute, Russian Academy of Science (LPI RAS), Moscow, Russia.

^b Università di Bari, Bari, Italy.

^c Università di Bologna, Bologna, Italy.

^d Università di Cagliari, Cagliari, Italy.

^e Università di Ferrara, Ferrara, Italy.

^f Università di Firenze, Firenze, Italy.

^g Università di Urbino, Urbino, Italy.

^h Università di Modena e Reggio Emilia, Modena, Italy.

ⁱ Università di Genova, Genova, Italy.

^j Università di Milano Bicocca, Milano, Italy.

^k Università di Roma Tor Vergata, Roma, Italy.

^l Università di Roma La Sapienza, Roma, Italy.

^m Università della Basilicata, Potenza, Italy.

ⁿ LIFAELS, La Salle, Universitat Ramon Llull, Barcelona, Spain.

^o Hanoi University of Science, Hanoi, Viet Nam.

^p Institute of Physics and Technology, Moscow, Russia.

^q Università di Padova, Padova, Italy.

^r Università di Pisa, Pisa, Italy.

^s Scuola Normale Superiore, Pisa, Italy.

^t Associated to Universidade Federal do Rio de Janeiro (UFRJ), Rio de Janeiro, Brazil.

^u Associated to Physikalisches Institut, Ruprecht-Karls-Universität Heidelberg, Heidelberg, Germany.

^v Associated to European Organization for Nuclear Research (CERN), Geneva, Switzerland.